Article

Journal of
Nanoscience and Nanotechnology
Vol. 16, 11823–11830, 2016
www.aspbs.com/jnn

Etching of Magnetic Tunnel Junction Materials Using Reactive Ion Beam

Min Hwan Jeon[1,†], Kyung Chae Yang[2,†], Jin Woo Park[2], Deok Hyun Yun[2], Kyong Nam Kim[3], and Geun Young Yeom[1,2,*]

[1] *SKKU Advanced Institute of Nano Technology (SAINT), Sungkyunkwan University, Suwon, Gyeonggi-do 440-746, South Korea*
[2] *Department of Advanced Materials Science and Engineering, Sungkyunkwan University, Suwon, Gyeonggi-do 440-746, South Korea*
[3] *School of Advanced Materials Science and Engineering, Daejeon University, Daejeon, 330-716, South Korea*

Magnetic tunnel junction (MTJ) materials such as CoPt, CoFeB, and MgO and the hard mask material such as W were etched with a reactive ion beam system using Ar, NF_3, CH_3OH, and CO/NH_3 as etch gases. The effects of etch gas and the energy of the ion beam on the etch characteristics were then investigated. When the MTJ materials were etched with an Ar ion beam, the etch selectivities of the MTJ materials over W and the etch profiles of the etched MTJ patterns masked with W were generally poor, possibly due to the nonselective etching, physical sputtering without chemical reaction, and severe redeposition of the nonvolatile etch residues on the sidewall of the etched features. The use of $NF_3 \rightarrow CH_3OH \rightarrow CO/NH_3$ reactive ion beam showed better etch selectivities over W and better etch profiles due to the higher etch selectivities of MTJ materials over W and less sidewall deposition. For reactive gases such as CH_3OH and CO/NH_3, the use of higher ion energy by increasing the 1st grid voltage of the ion beam up to +250 V also improved the MTJ etch profiles, possibly due to the increased effective chemical assisted physical sputtering of the etch products and the minimization of sidewall etch residues by removing etch products more effectively.

Keywords: Ion Beam Etching, Magnetic Tunnel Junction Materials, Reactive Ions, Chemical Assisted Physical Sputtering.

1. INTRODUCTION

Various non-volatile memory devices have been proposed as next generation memory devices to replace the existing memory devices due to their limited memory performances. Among these non-volatile memory devices, spin transfer torque magnetic random access memory (STT-MRAM) has been investigated as one of the promising candidates for next generation devices owing to its high density storage, low power consumption, high speed, etc.[1–5]

For the fabrication of nano-sized STT-MRAM devices, the precise etch control of MTJ normally consisting of CoFeB/MgO/CoFeB is essential for spin transfer torque switching and tunnel magnetoresistance (TMR).[6–8] Currently, the etching of MTJ-related materials using conventional reactive ion etching (RIE) methods incurs problems in STT-MRAM device fabrication such as low etch selectivity with hard mask, etch damage, and redeposition of etch residue on the sidewall of the etched MTJ feature, etc.[9–12] To alleviate these etch related problems during the etching of MTJ materials, many people have intensively investigated various methods to increase the volatility of etch residue during the etching, thus improving the etch characteristics of MTJ materials.[13–16] Various etch gases that possibly form volatile etch compounds with MTJ-related materials have been studied by some research groups to improve the etch selectivity and etch profile.[16–19] Other research groups have studied etch techniques such as pulse-biasing[20] and substrate heating[21] during etching in the RIE system to reduce the redeposited etch residue on the sidewall of the etched feature by increasing reactivity

*Author to whom correspondence should be addressed.
†These two authors contributed equally to this work.

and volatility with MTJ materials. For the substrate heating and bias pulsing, the researchers obtained both the improved etch selectivity of MTJ materials over W hard mask and improved MTJ etch profile with the increase of the substrate temperature and with the decrease of the pulse duty percentage, respectively.[22, 23]

Even though the RIE etch techniques investigated by many researchers described above improved the etch characteristics of MTJ materials, the non-volatile etch residue remained on the etched MTJ feature sidewall, resulting in a decrease of the device performance.[15, 24] Previously, ion beam etching (IBE) has been used for the etching of MTJ materials by using Ar ions; however, due to the lack of volatile compounds during the etching, heavily redeposited etch residue was observed on the surface and sidewall of the etched MTJ features when the MTJ pattern was not severely over-etched.[25–27] In this current study however, instead of an Ar ion beam, a reactive ion beam (RIB) etching system was investigated in the etching of MTJ materials to increase the volatility of etch residue formed during the etching with reactive gases. For the effective etching of MTJ patterns, various etch gases such as Ar, NF_3, CH_3OH, and CO/NH_3 gas mixture were used and their etch characteristics were analyzed.

2. EXPERIMENTAL DETAILS

The pattered MTJ stack was etched in a reactive ion beam system as shown in Figure 1. The reactive ion etching system was composed of an inductively coupled plasma (ICP)-type source for the plasma generation and three grids for the ion acceleration. 13.56 MHz rf power was applied to the ICP source and a positive voltage was applied to the first grid close to the plasma source to vary the ion beam energy. A negative voltage was applied to the second grid to focus the ion beam and to extract the ions from the source, and the third grid was grounded.

For the etch samples, to measure the etch rates, blank (or photoresist patterned) MTJ related materials such as CoPt, MgO, CoFeB, and W deposited on silicon wafers were used. For the nanoscale MTJ feature etching, a MTJ stack of CoPt (10 nm)/MgO (1 nm)/CoFeB (10 nm) deposited on a Ta (5 nm)/SiO_2/Si wafer and masked with a 40 nm width pattern composed of W(100 nm)/Ru(5 nm) was used. For the etch gases for the reactive ion beam etching, various etch gases such as Ar, NF_3, CH_3OH, and CO/NH_3(1:3) were used with the total gas flow rate of 80 sccm. The ICP source power of the reactive ion beam was kept at 300 W. The etch characteristics were observed as a function of the 1st grid voltage from +150 to +250 while keeping the second grid voltage at −300 V. The substrate temperature was kept at room temperature.

The etch depths of the MTJ materials and hard mask material for various etch gases were measured using a step profilometer (Tencor Alpha step 500). The etch profile of the patterned MTJ stack on a Ta/SiO_2/silicon wafer was observed by using a field emission scanning electron microscope (FE-SEM, Hitachi S-4700). The chemical binding states and composition of the MTJ pattern sidewall etched using various gases were examined by X-ray photoelectron spectroscopy (XPS, ESCA2000, VG Microtech Inc.) using a Mg K_α twin-anode source and the thickness of the etch residue and the residue composition remaining on the etched MTJ pattern sidewall were estimated. In particular, for more effective measurement of the chemical

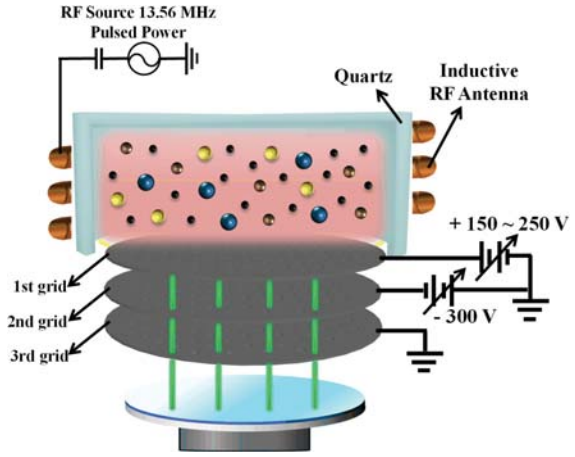

Figure 1. Schematic diagram of the reactive ion beam etching system used in this study. The reactive ion beam system was composed of an ICP-type ion gun with three grids. A power of 13.56 MHz rf was applied to the ICP source and a positive voltage from +150 V to +250 V was applied to the first grid for the acceleration of the ions extracted from the plasma source, a negative voltage of −300 V to the second grid to focus the ion beam, and the third grid was grounded.

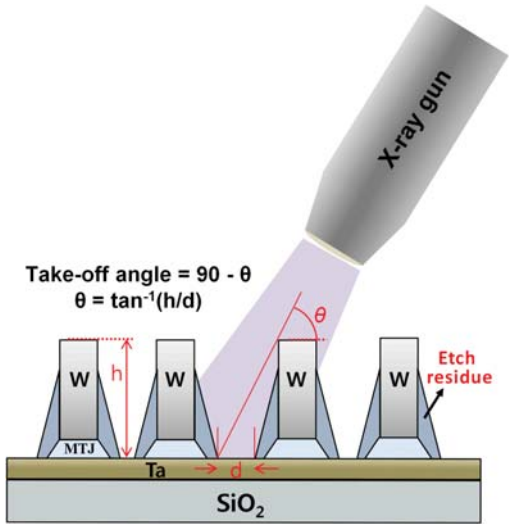

Figure 2. Schematic diagram of the XPS analysis technique used for the investigation of the etch residue redeposited on the sidewall of the nanoscale MTJ features. To measure the sidewall residue more effectively, a take-off angle of 20° was used as shown in the figure.

composition and thickness of the residue remaining on the etched MTJ feature, the XPS measurement was carried out with the take-off angle of 20° as shown in Figure 2.

3. RESULTS AND DISCUSSION

Using the ion beam etching system, the MTJ-related materials such as CoFeB, MgO, CoPt, and W were etched as a function of the 1st grid voltage from +150 to +200 (or +250) V and the measured etch rates are shown in Figures 3(a–d) for the different etch gases of Ar, NF_3, CH_3OH, and CO/NH_3, respectively. The ICP-type ion beam source power was maintained at 300 W and the second grid voltage was kept at −300 V while the 3rd grid was grounded. As shown in Figure 3(a), the increase of the 1st grid voltage from +150 to +200 V continuously increased the etch rates of all MTJ-related materials: CoFeB (from 0.89 to 1.41 nm/min), CoPt (from 0.99 to 1.58 nm/min), MgO (from 0.63 to 1.07 nm/min), W (from 0.26 to 0.65 nm/min). At a given 1st grid voltage, the etch rate was the highest for CoPt and it was followed by CoFeB → MgO → W. The differences in the etch rates at a given 1st grid voltage are believed to be related to the different sputter yields by Ar^+ ions. The etching with NF_3, CH_3OH, and CO/NH_3(1:3) at the total gas flow rate of 80 sccm shown in Figures 3(b–d), respectively, also exhibited similar etch trends by showing the increased etch rates of MTJ-related materials with the increase of the 1st grid voltage and by showing the lower etch rates in the sequence of CoPt (the highest etch rate), CoFeB, MgO, and W (the lowest etch rate). However, at a given 1st grid voltage, the use of NF_3 gas exhibited the highest etch rates of MTJ-related materials (CoFeB (from 1.14 to 1.92 nm/min), CoPt (from 1.31 to 2.34 nm/min), MgO (from 0.84 to 1.63 nm/min), and W (from 0.32 to 0.83 nm/min)) possibly due to the formation of more volatile etch compounds with fluorine in NF_3, due to the chemically assisted physical sputtering effect. In the case of CH_3OH and CO/NH_3, shown in Figures 3(c and d), respectively, even though chemically assisted physical sputtering is expected because of the forming of metal carbonyls ($M_x(Co)_y$) (possibly due to the formation of incomplete metal carbonyls and lower vapor pressure of the metal carbonyls), lower etch rates of materials were observed; that is, CoFeB (from 0.66 to 1.08 nm/min), CoPt (from 0.74 to 1.22 nm/min), MgO (from 0.47 to 0.83 nm/min), W (from 0.17 to 0.24 nm/min) for CH_3OH gas and CoFeB (from 0.68 to 1.24 nm/min), CoPt (from 0.83 to 1.4 nm/min), MgO (from 0.53 to 0.93 nm/min), and W (from 0.171 to 0.236 nm/min) for CO/NH_3 gas. The decrease of the etch rates with CH_3OH and CO/NH_3 could be improved by increasing the 1st grid voltage to +250 V.

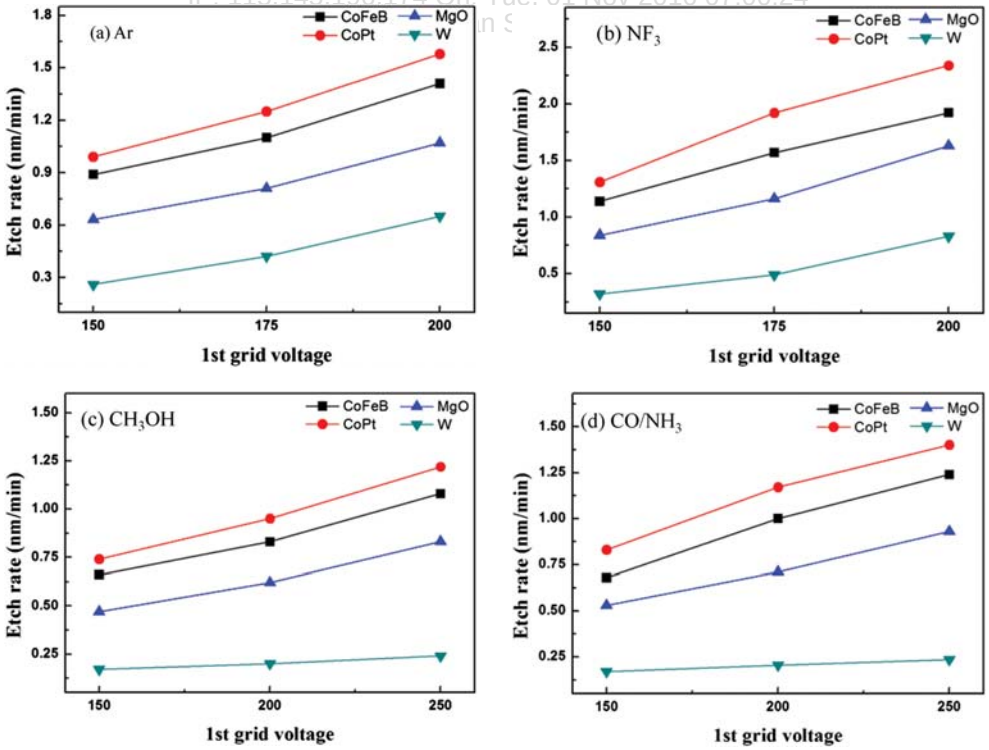

Figure 3. Etch rates of MTJ-related materials and W as a function of 1st grid voltage of an ion beam system for different etch gases of (a) Ar, (b) NF_3, (c) CH_3OH, and (d) CO/NH_3.

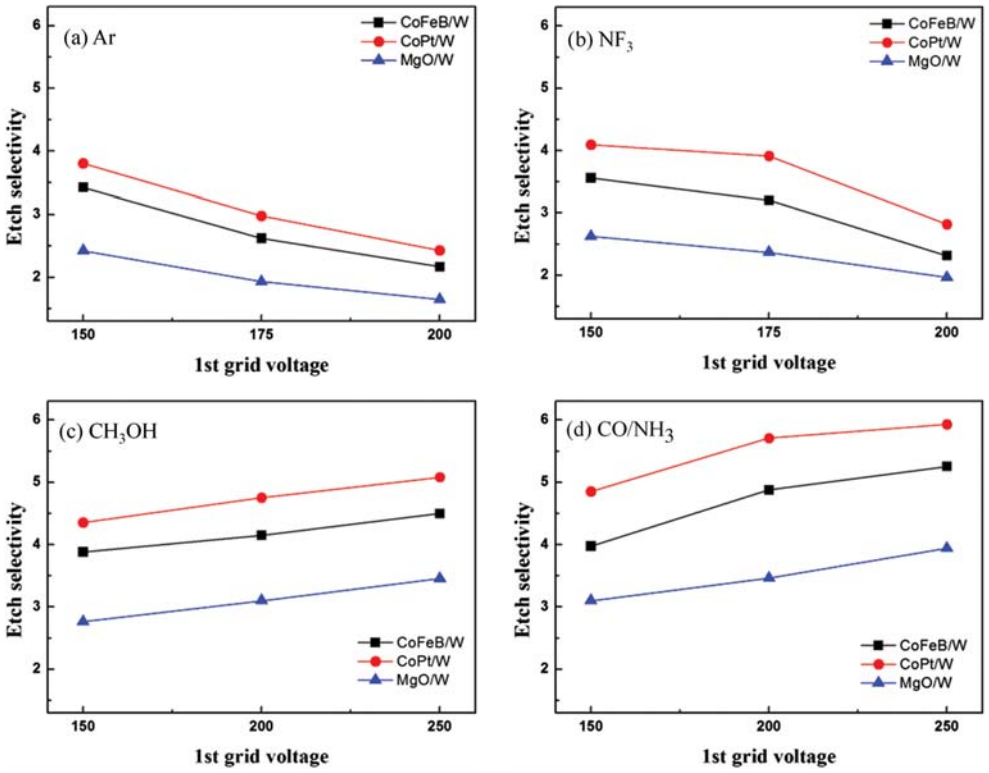

Figure 4. Etch selectivities of MTJ-related materials over W as a function of 1st grid voltage using (a) Ar, (b) NF_3, (c) CH_3OH, and (d) CO/NH_3 in an ion beam system.

Figures 4(a–d) exhibit the etch selectivities of CoFeB/W, CoPt/W, and MgO/W calculated as a function of the 1st grid voltage for Ar, NF_3, CH_3OH, and CO/NH_3 gas with the etch rates shown in Figure 3, respectively. As shown in Figures 4(a and b), the increase of the 1st grid voltage decreased the etch selectivities for Ar and NF_3, possibly due to the higher sputter yield of W and tungsten fluorides at a higher ion energy. In contrast, the etch selectivities increased with the increase of the 1st grid voltage and the use of CO/NH_3 exhibited higher etch selectivities than the CH_3OH: CoFeB/W (from 3.97 at +150 V to 5.25 at +250 V), CoPt/W (from 4.85 to 5.93), and MgO/W (from 3.09 to 3.94) as shown in Figures 4(c and d). The increase of etch selectivities with the increase of 1st grid voltage for CH_3OH and CO/NH_3 is believed to be related to the increased sputtering of the incomplete metal carbonyls formed by CH_3OH and CO/NH_3 at the higher ion energies.

Based on the results in Figures 3 and 4, nanoscale MTJ features composed of CoPt (10 nm)/MgO (1 nm)/CoFeB (10 nm) on a $Ta/SiO_2/Si$ wafer and masked with 40 nm width pattern composed of W(100 nm)/Ru(5 nm) were etched as a function of the 1st grid voltage for Ar, NF_3, CH_3OH, and CO/NH_3. The results are shown in

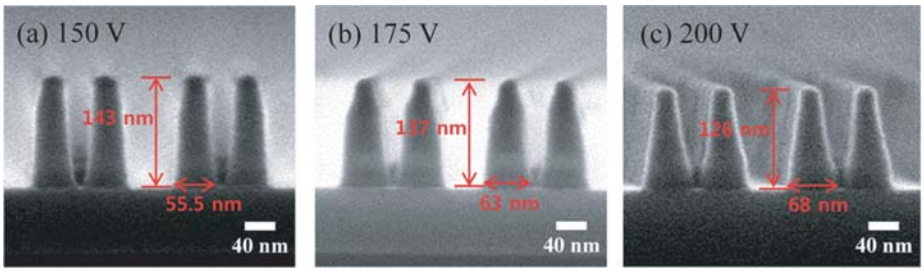

Figure 5. SEM images of the MTJ (CoPt/MgO/CoFeB) pattern on the W mask (W/Ti/Ru) etched using the Ar ion beam as a function of the 1st grid voltage from +150 V to +200 V. (a) +150 V, (b) +175 V, and (c) +200 V. The ion source was operated with 300 W of ICP power, −300 V of the second grid voltage, and the grounded third grid. Ar flow rate was 80 sccm and the samples were etched at room temperature.

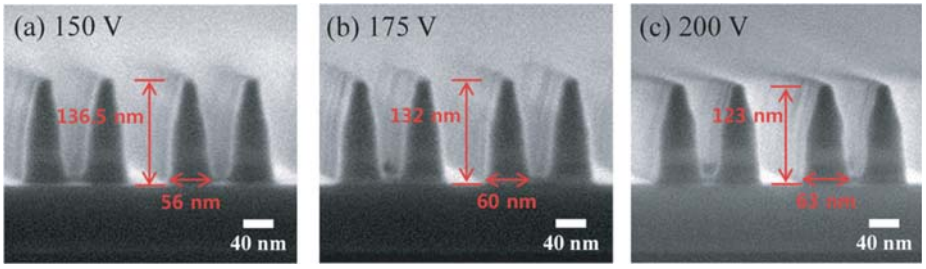

Figure 6. SEM images of the MTJ (CoPt/MgO/CoFeB) patterns etched using the NF_3 reactive ion beam as a function of 1st grid voltage from +150 V to +200 V. (a) +150 V, (b) +175 V, and (c) +200 V. Other process conditions are maintained the same as those in Figure 5.

Figures 5–8, respectively. With Ar gas, as shown in Figures 5(a–c) for the 1st grid voltage of +150, +175, and +200 V, respectively, the increase of the 1st grid voltage degraded the W mask on the MTJ feature and increased the feature bottom width from 55.5 nm at +150 V to 68 nm at +200 V after the etching of the MTJ layer. This indicates that more etch residue was redeposited on the sidewall of the etched feature. When the nanoscale MTJ features were etched with NF_3 instead of Ar, as shown in Figure 6, the increase of the 1st grid voltage degraded the W hardmask and increased the bottom width of the MTJ feature, similar to the cases for Ar. However, the bottom width of the features after the etching of the MTJ layer was thinner, possibly due to the higher vapor pressure of the metal fluorides compared to that of metal atom itself. On the contrary, when CH_3OH and CO/NH_3 were used as the etch gases, as shown in Figures 7 and 8, the increase of the 1st grid voltage did not degrade the W hardmask, but instead decreased the bottom width of the MTJ features. Therefore, the MTJ etch profiles were improved and the etch residue on the sidewall of the MTJ feature was decreased with the increase of ion energy, possibly due to the high etch selectivities and the increased volatility of the metal carbonyls formed on the MTJ surface during the etching at the higher ion energy. In addition, the use of CO/NH_3 exhibited a thinner bottom width of the MTJ features at the same 1st grid voltage, indicating a more anisotropic etch profile and less sidewall residue possibly due to more volatile metal carbonyl formation compared to CH_3OH during the etching.

The binding states of the etch residue redeposited on the sidewall of the etched MTJ features were investigated using XPS at the take-off angle of 20°. This was carried out to more effectively measure the etch residue remaining on the nanoscale MTJ etched feature. The results are shown in Figures 9(a–d) for Co $2p$, Fe $2p$, Pt $4f$, and W $4f$, respectively. For Ar and NF_3, +150 V of the 1st grid voltage was used, and for CH_3OH and CO/NH_3, +250 V was used. Other etch conditions were maintained the same as those in Figures 5∼8. Pure metal peaks were observed at 778.3 ($2p_{3/2}$) and 793.1 ($2p_{1/2}$) eV for Co, 707.1 eV ($2p_{3/2}$) and 720.2 eV ($2p_{1/2}$) for Fe, 71.1 eV ($4f_{7/2}$) and 74.5 ($4f_{5/2}$) eV for Pt, and 31.4 ($4f_{7/2}$) and 33.4 ($4f_{5/2}$) eV for W. *B* peaks were also observed but their intensities were very low. For etching using Ar, CH_3OH, and CO/NH_3, metal oxide related peaks were observed at higher binding energies than for the metal peaks, at 780.9 and 796.9 eV for Co–O_x, 710 and 723.7 eV for Fe–O_x, 72.3 and 77.1 eV for Pt–O_x, and 35.6 and 37.8 eV for W–O_x. For etching using NF_3, metal fluoride related peaks with the highest binding energies were observed at 782.7 and 798.1 eV for Co–F_x, 711.4 and 724.8 eV for Fe–F_x, 72.9 and 78.8 eV for Pt–F_x, and 36.5 and 38.8 eV for W–F_x. As shown in Figure 9, the highest etch residue peak intensities related to oxides were observed for the etching using Ar and the oxide related peak intensities were lower for etching using CH_3OH, and the lowest oxide related peak intensities were observed for etching using CO/NH_3. For NF_3 etched MTJ features, instead of oxide related peaks, high metal fluoride related

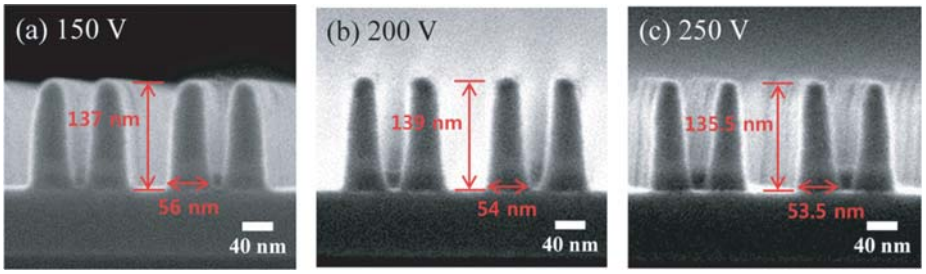

Figure 7. SEM images of the MTJ (CoPt/MgO/CoFeB) patterns etched using the CH_3OH reactive ion beam as a function of 1st grid voltage from +150 V to +250 V. (a) +150 V, (b) +200 V, and (c) +250 V. Other process conditions are maintained the same as those in Figure 5.

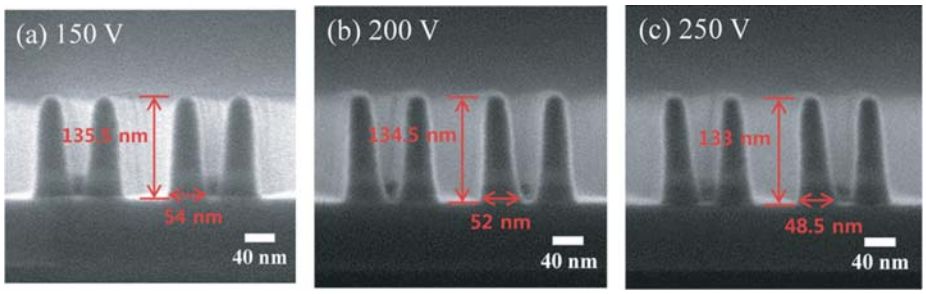

Figure 8. SEM images of the MTJ (CoPt/MgO/CoFeB) patterns etched using the CO/NH_3 reactive ion beam as a function of 1st grid voltage from +150 V to +250 V. (a) +150 V, (b) +200 V, and (c) +250 V. Other process conditions are maintained the same as those in Figure 5.

peak intensities were observed due to the etch residue redeposited on the sidewall of the MTJ etched feature. Figure 9 also shows the metal peak intensities that could have originated from the etched MTJ feature itself rather than from the etch residue redeposited on the sidewall of the etched MTJ features. As shown in Figure 9, the pure metal peak intensities were lower for the etching using Ar, but the intensities were increased for the etching using NF_3. Also, a further increase of metal peak intensities was observed for the etching using CH_3OH and the highest metal peak intensities for CO/NH_3.

Using the XPS results shown in Figure 9, the relative atomic percentages of the etched MTJ feature sidewall among Co, Fe, B, Pt, and W were investigated for different etch gases of Ar, NF_3, CH_3OH, and CO/NH_3 and the results are shown in Figure 10. As shown in Figure 10, the MTJ feature etched using Ar gas exhibited the highest percentages of Co, Fe, B, and Pt and the lowest percentage of W. Also, the use of NF_3, CH_3OH, and CO/NH_3 consecutively exhibited the lower percentages of Co, Fe, B, and Pt and the higher percentage of W. The components such as Co, Fe, B, and Pt could be more closely related to

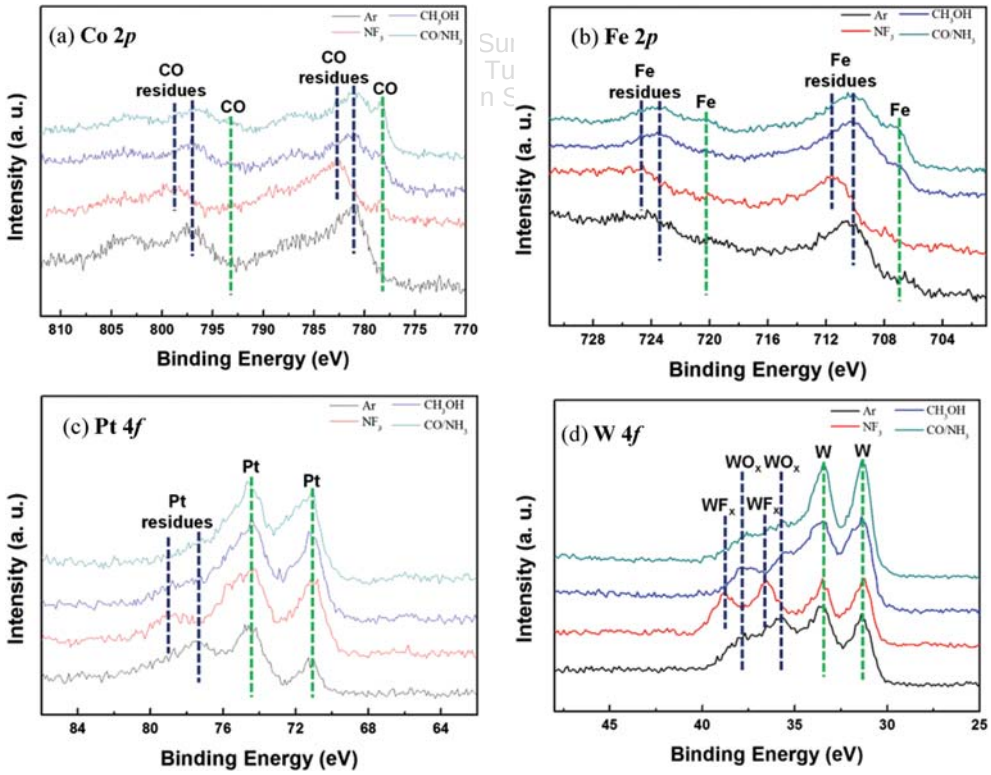

Figure 9. XPS narrow scan data of Co 2*p*, Fe 2*p*, Pt 4*f*, and W 4*f* on the etched MTJ pattern sidewall with various etch gases of Ar, NF_3, CH_3OH, and CO/NH_3 while keeping the 1st grid voltage at +150 V for the etching with Ar and NF_3 gas and at +250 V for the etching with CH_3OH and CO/NH_3. (a) Co 2*p*, (b) Fe 2*p*, (c) Pt 4*f*, and (d) W 4*f*. The etched MTJ pattern sidewall was investigated using a Mg $K\alpha$ twin-anode source and a 20° tilted angle.

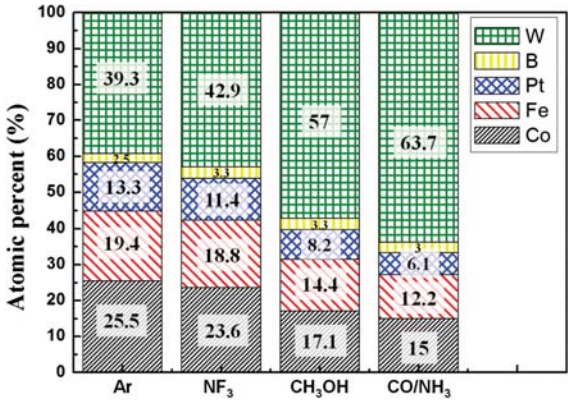

Figure 10. Relative atomic percentages of the etched MTJ pattern sidewall materials measured by XPS for different etch gases.

the etch residue redeposited on the sidewall of the etched MTJ features (these signals could be originated not only from the etched MTJ feature surface but also from the etch residue redeposited on the sidewall of the feature), while the W component is more closely related to the original MTJ feature (W is the patterned hard mask). The higher W percentage is related to the thinner etch residue redeposited on the sidewall of the etched MTJ feature. Therefore, the etch residue redeposited on the sidewall of the etched MTJ features appeared to be lower in sequence for the etching with Ar (thickest), NF_3, CH_3OH, and CO/NH_3 (thinnest).

4. CONCLUSION

For a more selective and more anisotropic etching of a nanoscale MTJ stack with less sidewall residue for STT-MRAM devices, MTJ-related materials and W hard mask material were etched using a three-grid ion beam etching system with reactive etch gases such as NF_3, CH_3OH, and CO/NH_3. In addition, Ar and the etch characteristics of MTJ-related materials as well as nanoscale MTJ patterned with W were investigated. At a given 1st grid voltage, the use of CH_3OH and CO/NH_3 exhibited higher etch selectivities compared to the use of Ar and NF_3, even though the etch rates of MTJ materials were lower. Also, higher etch selectivities in addition to the higher etch rates could be obtained at the higher 1st grid voltage for CH_3OH and CO/NH_3, while Ar and NF_3 exhibited lower etch selectivities at the higher 1st grid voltage, even though the etch rates of the MTJ materials were higher. The differences in etch characteristics is believed to be related to the chemically assisted sputter characteristics of the etch compounds such as metal carbonyls for CH_3OH and CO/NH_3 and metal fluorides for NF_3. When the MTJ layer (CoPt/MgO/CoFeB) patterned with 40 nm scale W hardmask was etched with Ar, NF_3, CH_3OH, and CO/NH_3, the MTJ etch profiles were degraded with the increase of the 1st grid voltage for Ar and NF_3 due to the lower etch selectivities at the higher 1st grid voltage. On the contrary, the MTJ etch profiles were improved for CH_3OH and CO/NH_3 with increasing 1st grid voltage, possibly because of the higher etch selectivities at the higher 1st grid voltage through the improved chemically assisted physical sputtering of the metal carbonyls formed on the MTJ surface. The etch residue redeposited on the sidewall of the etched MTJ features was lower for the etching using CH_3OH and CO/NH_3 than those etched with Ar and NF_3. Comparing CH_3OH and CO/NH_3, the lower etch residue was observed for the CO/NH_3, possibly due to the formation of more stable and more volatile metal carbonyl formation compared to CH_3OH. Therefore, the most anisotropic MTJ etch profiles with the least etch residue deposited on the sidewall of the etched MTJ feature could be observed with the reactive ion beam etching using CO/NH_3.

Acknowledgments: This work was supported by the Industrial Strategic Technology Development Program (10041681, Development of fundamental technology for 10 nm process semiconductor and 10 G size large area process with high plasma density and VHF condition) founded by the Ministry of Knowledge Economy (MKE, Korea).

References and Notes

1. D. C. Worledge, G. Hu, D. W. Abraham, J. Z. Sun, P. L. Trouilloud, J. Nowak, S. Brown, M. C. Gaidis, E. J. O'Sullivan, and R. P. Robertazzi, *Appl. Phys. Lett.* 98, 022501 **(2011)**.
2. S. Mangin, D. Ravelosona, J. A. Katine, M. J. Carey, B. D. Terris, and E. E. Fullerton, *Nature Mater.* 5, 210 **(2006)**.
3. A. Driskill-Smith, S. Watts, V. Nikitin, D. Apalkov, D. Druist, R. Kawakami, X. Tang, X. Luo, A. Ong, and E. Chen, *Proc. Int. Symp.*, VLSI Technology, Hsinchu, Taiwan **(2010)**, p. 51.
4. D. Apalkov, A. Khvalkovskiy, S. Watts, V. Nikitin, X. Tang, D. Lottis, K. Moon, X. Luo, E. Chen, A. Ong, A. Driskill-Smith, and M. Krounbi, *ACM J. Emerg. Technol. Comput. Syst.* 9, 13 **(2013)**.
5. K. Ueda, T. Koyama, D. Chiba, K. Shimamura, H. Tanigawa, S. Fukami, T. Suzuki, N. Ohshima, N. Ishiwata, Y. Nakatani, and T. Ono, *Appl. Phys. Express* 4, 063003 **(2011)**.
6. H. Kubota, S. Ishibashi, T. Saruya, T. Nozaki, A. Fukushima, K. Yakushiji, K. Ando, Y. Suzuki, and S. Yuasa, *J. Appl. Phys.* 111, 07C723 **(2012)**.
7. W. H. Butler, X.-G. Zhang, T. C. Schulthess, and J. M. MacLaren, *Phys. Rev. B* 63, 054416 **(2001)**.
8. J. Mathon and A. Umerski, *Phys. Rev. B* 63, 220403 **(2001)**.
9. K. Sugiura, S. Takahashi, M. Amano, T. Kajiyama, M. Iwayama, Y. Asao, N. Shimomura, T. Kishi, S. Ikegawa, H. Yoda, and A. Nitayama, *Jpn. J. Appl. Phys.* 428, 08HD02 **(2009)**.
10. X. Peng, S. Wakeham, A. Morrone, S. Axdal, M. Feldbaum, J. Hwub, T. Boonstra, Y. Chen, and J. Ding, *Vacuum* 83, 1007 **(2009)**.
11. T. Y. Lee, I. H. Lee, and C. W. Chung, *Thin Solid Films* 547, 146 **(2013)**.
12. T. Kanazawa, S.-I. Motoyama, T. Wakayama, and H. Akinaga, *J. Magn. Magn. Mater.* 12, 81 **(2007)**.
13. Y. B. Xiao, E. H. Kim, S. M. Kong, and C. W. Chung, *Thin Solid Films* 519, 8229 **(2011)**.
14. N. Matsui, K. Mashimo, A. Egami, A. Konishi, O. Okada, and T. Tsukada, *Vacuum* 66, 479 **(2002)**.

15. K. Kinoshita, H. Utsumi, K. Suemitsu, H. Hada, and T. Sugibayashi, *Jpn. J. Appl. Phys.* 49, 08JB02 **(2010)**.

16. T. Osada, M. Doi, K. Sakamoto, H. Maehara, and Y. Kodaira, *Proc. 26th. Int. Symp. Dry Process (DPS)*, Tokyo, Japan **(2004)**, p. 127.

17. H. Maehara, T. Osada, M. Doi, K. Sakamoto, K. Tsunekawa, D. D. Djayaprawira, Y. Kodaira, N. Watanabe, H. Kubota, A. Fukushima, Y. Otani, S. Yuasa, and K. Ando, *Dig. IEEE Intermag. Conf.*, Nagoya, Japan **(2005)**, p. 1535.

18. K. B. Jung, J. Hong, H. Cho, S. Onishi, D. Johnson, Y. D. Park, J. R. Childress, and S. J. Pearton, *J. Vac. Sci. Technol. A* 17, 535 **(1999)**.

19. I. H. Lee, T. Y. Lee, and C. W. Chung, *Vacuum* 97, 49 **(2013)**.

20. M. H. Jeon, H. J. Kim, K. C. Yang, S.-K. Kang, K. N. Kim, and G. Y. Yeom, *Jpn. J. Appl. Phys.* 52, 05EB03 **(2013)**.

21. M. Lee and W. J. Lee, *Appl. Surf. Sci.* 258, 8100 **(2012)**.

22. M. H. Jeon, D. H. Yun, K. C. Yang, J. Y. Youn, D. Y. Lee, T. H. Shim, J. G. Park, and G. Y. Yeom, *J. Nanosci. Nanotechnol.* 14, 9680 **(2014)**.

23. K. C. Yang, M. H. Jeon, and G. Y. Yeom, *Jpn. J. Appl. Phys.* 54, 01AE01 **(2015)**.

24. K. Kinoshita, K. Suemitsu, N. Ohshima, N. Ishiwata, and T. Sugibayashi, *Proc. 63rd GEC/7th ICRP/28th SPP*, Paris, France **(2010)**, KWP-00067.

25. S. W. Chun, D. H. Kim, J. H. Kwon, B. H. Kim, S. J. Choi, and S. B. Lee, *J. Appl. Phys.* 111, 07C722 **(2012)**.

26. T. J. Kropewnicki, A. M. Paterson, T. Panagopoulos, and J. P. Holland, *J. Vac. Sci. Technol. A* 24, 444 **(2006)**.

27. S. Takahashi, T. Kai, N. Shimomura, T. Ueda, M. Amano, M. Yoshikawa, E. Kitagawa, Y. Asao, S. Ikegawa, T. Kishi, H. Yoda, K. Nagahara, T. Mukai, and H. Hada, *IEEE Trans. Magn.* 42, 2745 **(2006)**.

Received: 4 January 2016. Accepted: 1 March 2016.